Weierstraß-Institut
für Angewandte Analysis und Stochastik

im Forschungsverbund Berlin e.V.

Preprint ISSN 0946 – 8633

Stochastic flow simulation and particle transport in a 2D layer of random porous medium

O.A. Kurbanmuradov[1] and K.K. Sabelfeld[2,3]

[1] Centre for Phys. Math. Research at Turkmen State University,
Saparmyrat Turkmenbashy av. 31, Ashgabad, Turkmenistan
E-mail: Kurbanmuradov@yandex.ru

[2] Weierstrass Institute for Applied Analysis and Stochastics
Mohrenstr. 39, 10117 Berlin, Germany
E-Mail: sabelfel@wias-berlin.de

[3] Institute of Computational Mathematics
and Mathematical Geophysics, Russian Acad. Sci.
Lavrentieva str., 6, 630090 Novosibirsk, Russia

No. 1374
Berlin 2008

2000 *Mathematics Subject Classification.* 65C05, 65C20, 76S05,
PACS: 02.60.Cb, 02.70.Lq .

Key words and phrases. Darcy equation, random hydraulic conductivity, Randomized spectral models, diffusion regime, long-range correlations .

The first author acknowledges the WIAS Institute, Berlin, for the support and hospitality during his 2 months stay in Berlin. Support of the RFBR Grant N 06-01-00498 is acknowledged by the second author.

Edited by
Weierstraß-Institut für Angewandte Analysis und Stochastik (WIAS)
Mohrenstraße 39
10117 Berlin
Germany

Fax: + 49 30 2044975
E-Mail: preprint@wias-berlin.de
World Wide Web: http://www.wias-berlin.de/

Abstract

A stochastic numerical method is developed for simulation of flows and particle transport in a 2D layer of porous medium. The hydraulic conductivity is assumed to be a random field of a given statistical structure, the flow is modeled in the layer with prescribed boundary conditions. Numerical experiments are carried out by solving the Darcy equation for each sample of the hydraulic conductivity by a direct solver for sparse matrices, and tracking Lagrangian trajectories in the simulated flow. We present and analyze different Eulerian and Lagrangian statistical characteristics of the flow such as transverse and longitudinal velocity correlation functions, longitudinal dispersion coefficient, and the mean displacement of Lagrangian trajectories. We discuss the effect of long-range correlations of the longitudinal velocities which we have found in our numerical simulations. The related anomalous diffusion is also analyzed.

1 Introduction

The main difficulty in evaluation of pollutant transport in porous medium (e.g., in aquifers, filters, bio-materials, e.g., see [2], [7], [24]) is the extreme heterogeneity of the media. This is a classical situation where there is a lack of knowledge about the local details of the spatial structure, but without this structure details, it is no chance to describe the large scale behavior. A natural approach is based on a stochastic description, where the heterogeneities are modeled as random fields with given statistical properties (e.g., see [1]-[4]). In hydrology the stochastic approach is often used for the flow analysis in saturated zone (e.g., see [6], [22]).

In the flow simulation through a porous medium, one uses in the hydrology an Ansatz experimentally well supported that the hydraulic conductivity can be considered as a random field with a lognormal distribution. To analyze the Darcy equation with the random hydraulic conductivity in the case when its intensity of fluctuations is small, one applies the small perturbation method. We are aware of two versions of this method. The first version deals mainly with the means and variances, thus estimating only some deterministic scales of the process see (e.g., see [2], [7]). The second version takes into account the spectral structure of the random solution, and thus it is able to construct samples of the random solutions and to evaluate practically arbitrary statistical characteristics of the solution (e.g., see [18], [21]). But since this approach works under the assumption of small fluctuation intensities, only a Gaussian approximation to the solution field is possible.

The case of large fluctuations is much more difficult, and can be treated by solving numerically the Darcy equation, say, by a finite difference or finite element methods, often called also stochastic finite element methods, e.g., see [1], [25], [8].

We mention also the polynomial chaos expansion approach, a method in which it is attempted to reduce the original stochastic boundary value problem to a series of deterministic equations (e.g., see [27], [28], [29]). This method however is applicable only if a small number of terms in the series expansion is sufficient for a good approximation which is rather rare in practice.

Important class of this type of methods is the Karhunen-Loève expansion. Generally, it is computational demanding because it requires to solve numerically eigen-value problems of high dimension. However in some practically interesting cases models with analytically solvable eigen-value problem for the correlation operator can be obtained. This gives then a very efficient numerical method because as a rule, the K-L expansions are fast convergent. An exactly solvable case for the viscous flow simulation with random excitations of the velocities prescribed on the boundary is given in the recent paper by K. Sabelfeld [17].

We develop in the present paper a direct stochastic simulation method which consists in a direct numerical construction of an ensemble of solutions to the Darcy equation with the relevant samples of the hydraulic conductivity. The random field of the hydraulic conductivity is simulated by the Monte Carlo Randomization Spectral algorithm, the finite-difference system approximating the Darcy equation is solved by a direct sparse matrix inversion, and the transport of particles is modeled by tracking the Lagrangian trajectories in the simulated velocity samples. It should be noted that the direct inversion methods are very robust in this problem where the equation coefficients are highly heterogeneous, but the main problem is to find an efficient solver for the relevant linear systems. This is done in the present paper by using the sparse structure of the relevant finite-difference system of equations.

The problem of evaluation of the diffusion regime is computationally very intensive since the transport should be simulated for thousands of correlation length scales (e.g., see [21], [5]). Therefore the problem was studied only with the first order approximation ([21], [4], [23]) which is applicable under strong restrictions of small fluctuations of the log conductivity. In the long-range transport most interesting is the case of large fluctuations. To our knowledge, there is only one study [5] where the general case of large fluctuations was considered, and the long-range transport was studied numerically for more than thousands of correlation length scales. In this study, a 2D flow was simulated by an iterative multigrid method where the transport was evaluated up to 1638 correlation length scales, but in this model, the dispersion coefficient was defined by averaging over a discrete cloud of particles moving in one fixed sample of the flow. This is different from the averaging over an ensemble of Lagrangian trajectories starting from a fixed point. As to the interrelation of these two definitions, see e.g., [21], [5], [23].

We focus on the existence of a diffusion regime in the longitudinal dispersion, and study the long-range transport and mixing of particles in layers with a length of thousands of log conductivity correlation lengths. We present a numerical analysis of different Eulerian and Lagrangian statistical characteristics of the flow such as transverse and longitudinal velocity correlation functions, the diffusion coefficient, the mean displacement of Lagrangian particles, and the probability density function of the transverse Lagrangian coordinate.

2 Simulation of flow and transport

2.1 Setting of the problem

We deal in this paper with the flow simulation and particle transport in a porous 2D layer which is considered as a rectangular domain $D = [0, L_x] \times [0, L_y]$ of finite size. The hydraulic conductivity $K(\mathbf{x})$, $\mathbf{x} = (x, y) \in D$ is assumed to be a lognormal random field with a given correlation function.

We consider a stationary flow in a saturated porous media governed by the Darcy law

$$\mathbf{q}(\mathbf{x}) = \theta(\mathbf{x})\mathbf{v}(\mathbf{x}) = -K(\mathbf{x})\nabla(\phi(\mathbf{x})) \tag{1}$$

where $\mathbf{q}$ is the Darcy velocity, or the specific discharge, $\mathbf{v}$ is the pore velocity, θ, the porosity, ϕ, the hydraulic head $\phi = z + p/(g\rho)$, ρ, the fluid density, g, the standard gravity, z is the elevation height. Fixed head conditions at the left and right boundaries and no flow conditions on the up and bottom boundaries of the layer D are assumed. This leads to a uni-directional velocity trend (mean velocity) which is horizontal, i.e., parallel to the OX axis. Therefore we call x a longitudinal, or horizontal, and y transverse, or vertical coordinates, respectively.

The functions θ and K are the key parameters of the flow. Experimental measurements show a high heterogeneous behavior of K in space with the following remarkable property: when considering K as a random field, its distribution is well approximated by the log-normal law (e.g., see [2], [7]). Therefore, in models, the hydraulic log conductivity $Y = \ln K$ is commonly considered as a statistically homogeneous random field. Let us denote the fluctuation of Y by $Y' = Y - \langle Y \rangle$, and let $B_Y(\mathbf{r}) = \langle Y'(\mathbf{x}+\mathbf{r})Y'(\mathbf{x})\rangle$ be the correlation function of the hydraulic log conductivity. Here and throughout the paper the angle brackets stand for the expectation over the relevant distribution of the random field Y, and the prime sign stands to indicate the fluctuation part.

The porosity θ is considered in some models also as a random field. However its variability is generally much smaller than that of K, and it is assumed to be constant in our study.

2.2 The Darcy equation

We will assume that there are no sources or sinkes in D, so $\nabla \cdot \mathbf{q} = 0$. Since the porosity is constant, the velocity field $\mathbf{v}(\mathbf{x}) = (u(x,y), v(x,y)))$ obeys

$$\frac{\partial u}{\partial x} + \frac{\partial v}{\partial y} = \nabla \cdot \mathbf{v}(\mathbf{x}) = \nabla \cdot \left(\frac{\mathbf{q}(\mathbf{x})}{\theta} \right) = 0, \tag{2}$$

i.e., the flow is divergence free. Thus the coupled system (1)-(2) yields the second order elliptic equation for the hydraulic head:

$$\frac{\partial}{\partial x}\left(K(x,y)\frac{\partial \phi}{\partial x} \right) + \frac{\partial}{\partial y}\left(K(x,y)\frac{\partial \phi}{\partial y} \right) = 0 \ . \tag{3}$$

Concerning the behaviour at the boundaries, we assume no flow boundary conditions on the up and bottom borders of the layer D, i.e.,

$$\frac{\partial \phi}{\partial y}(x,0) = \frac{\partial \phi}{\partial y}(x,L_y) = 0, \quad x \in (0,L_x). \tag{4}$$

On the left and right ends of the layer D, fixed head boundary conditions are prescribed

$$\phi(0,y) = 0, \quad \phi(L_x,y) = -J \cdot L_x, \quad y \in (0,L_y), \tag{5}$$

where $J > 0$ is a dimensionless constant.

We assume throughout the paper that the log conductivity $Y(\mathbf{x}) = \ln K(\mathbf{x})$ is an isotropic Gaussian random field. Two typical variants of correlation functions $B_Y(\mathbf{r}) = \langle Y'(\mathbf{x}+\mathbf{r})Y'(\mathbf{x})\rangle$ are: *the Gaussian correlation function* (e.g., see [26], [4]):

$$B_Y(\mathbf{r}) = \sigma_Y^2 \exp\Big(-\frac{|\mathbf{r}|^2}{\lambda^2} \Big) \ , \tag{6}$$

and *the exponential correlation function* [5], [19]:

$$B_Y(\mathbf{r}) = \sigma_Y^2 \exp\Big(- \frac{|\mathbf{r}|}{\lambda} \Big) \ , \tag{7}$$

where λ is the log conductivity correlation length scale.

It is convenient to choose the following dimensionless variables

$$\tilde{\mathbf{x}} = \frac{\mathbf{x}}{\lambda}, \quad \tilde{\mathbf{v}} = \frac{\theta \mathbf{v}}{K_G J}, \quad \tilde{\phi} = \frac{\phi}{J\lambda},$$

where $K_G = e^{\langle Y \rangle}$.

Hence, $\tilde{\mathbf{v}}(\tilde{\mathbf{x}})$ solves the problem (2)-(5), where the following changes have do be made: $\mathbf{x}$ is changed with $\tilde{\mathbf{x}}$, take $J = 1$, change L_x and L_y with the dimensionless variables $\tilde{L}_x = L_x/\lambda$ and $\tilde{L}_y = L_y/\lambda$; in addition, the log conductivity field Y should be taken so that $\langle Y \rangle = 0$ with the correlation function (6) or (7) having the dimensionless correlation length scale $\lambda = 1$. The dimensional velocity is then recovered by

$$\mathbf{v}(\mathbf{x}) = \frac{K_G J}{\theta} \tilde{\mathbf{v}}(\mathbf{x}/\lambda). \tag{8}$$

Note that when dealing with the transport problem, we track the particles by solving the evolution equation where we choose the dimensionless time

$$\tilde{t} = \frac{K_G J}{\lambda \theta} t.$$

Remark. In what follows we use throughout the paper the dimensionless variables only, so we omit the sign $\tilde{\cdot}$.

2.3 Finite-difference approximation

Let us introduce a uniform grid in our domain D by $x_i = (i-1)h_x$, $i = 1, ..., N_x$, $h_x = L_x/(N_x - 1)$; $y_j = (j-1)h_y$, $j = 1, ..., N_y$, $h_y = L_y/(N_y - 1)$. Denote $x_{i+1/2} = x_i + h_x/2$, $i = 1, ..., N_x - 1$; $y_{j+1/2} = y_j + h_y/2$, $j = 1, ..., N_y - 1$. We use the following conservative finite-difference approximation of the Darcy equation (1)-(2) with the boundary conditions (4)-(5) [20]:

$$\frac{u_{i+1/2,\,j} - u_{i-1/2,\,j}}{h_x} + \frac{v_{i,\,j+1/2} - v_{i,\,j-1/2}}{h_y} = 0, \quad i = 2, ..., n_x, \ j = 2, ..., n_y; \tag{9}$$

$$\frac{u_{i+1/2,\,j} - u_{i-1/2,\,j}}{h_x} + \frac{2\, v_{i,\,j+1/2}}{h_y} = 0, \quad i = 2, ..., n_x; \ j = 1; \tag{10}$$

$$\frac{u_{i+1/2,\,j} - u_{i-1/2,\,j}}{h_x} - \frac{2\, v_{i,\,j-1/2}}{h_y} = 0, \quad i = 2, ..., n_x; \ j = N_y; \tag{11}$$

$$\phi_{1,\,j} = 0, \quad \phi_{N_x,\,j} = -J\, L_x, \quad j = 1, ..., N_y \ , \tag{12}$$

where we use the notation $n_x = N_x - 1$, $n_y = N_y - 1$. Here the velocity components in the grid points $(x_{i+1/2}, y_j)$ and $(x_i, y_{j+1/2})$ are

$$u_{i+1/2,\,j} = -K_{i+1/2,\,j}\frac{\phi_{i+1,\,j} - \phi_{i,\,j}}{h_x}, \quad i = 1, ..., n_x;\ j = 1, ..., N_y; \tag{13}$$

$$v_{i,\,j+1/2} = -K_{i,\,j+1/2}\frac{\phi_{i,\,j+1} - \phi_{i,\,j}}{h_y}, \quad i = 1, ..., N_x;\ j = 1, ..., n_y \tag{14}$$

where ϕ_{ij} are the values of the head function ϕ in the points (x_i, y_j), and $K_{i+1/2,\,j}$ and $K_{i,\,j+1/2}$ are the values of the hydraulic conductivity in points $(x_{i+1/2}, y_j)$ and $(x_i, y_{j+1/2})$, respectively. Substituting of the equations (13) and (14) in the system (9)- (12) yields a system of $N = N_x\, N_y$ linear equations for the unknowns ϕ_{ij}.

It should be noted that generally, when the hydraulic conductivity and the head function are smooth enough, the solution $\phi_{i,\,j}$ of the system of linear equations (9)-(12) approximates the true solution $\phi(x_i, y_j)$ to within the approximation error of order $O(h_x^2 + h_y^2)$. In practical problems however, when the hydraulic conductivity field is not smooth enough, the order of this approximation can be lower.

The obtained linear system of equations (9)-(12) can be solved by different iteration methods, e.g., the conjugate gradient methods, SOR, Krylov subspace projections, etc. However in this problem, the iterative methods are generally slowly convergent (e.g., see [5], [26]). Iterative methods of multigrid type are often efficient, well-suited to regular grids, but sensitive to condition number. Note that the condition number in this problem is rapidly increasing with the increase of the variance of the log conductivity, e.g., see [5].

Direct methods are highly efficient but require a large memory space. We however use the sparse structure of the system of equations, and apply direct linear solvers for sparse matrices.

The choice of the discretization step h is not trivial since it depends on the smoothness of samples of the coefficient K. For instance, the case when the correlation function of the log conductivity is Gaussian, the samples are smooth enough, and our experiments show that the step $h = 0.2$ is already enough to ensure that the relative error is about of 1% when calculating the one- and two-point statistical characteristics of the Eulerian velocity. For the exponential correlation function, the step should be taken at least two times less, to provide the same accuracy.

To construct the sample functions of the hydraulic conductivity we use the Randomization spectral method (e.g., see [10], [13], [16]), thus the simulation formula for the hydraulic conductivity is $K(x, y) = K_G\, e^{Y'(x,y)}$ where $Y'(x, y)$ is simulated according to the formula (24) presented in the Appendix,

$$Y'(x, y) = \frac{\sigma_Y}{\sqrt{n_0}} \sum_{j=1}^{n_0} (\xi_j \cos\tilde{\theta}_j + \xi'_j \sin\tilde{\theta}_j)\ , \tag{15}$$

where $\tilde{\theta}_j = \sqrt{2}(\eta_j x + \eta'_j y)$. In calculations, n_0, the number of retained terms in (15) should be chosen carefully since this choice has an essential impact on the simulation results. Indeed, if n_0 is not large enough, the distribution of the simulated random field Y' may considerably deviate from the Gaussian one. In addition, this leads to ignoring the influence of small spatial scales of Y'. Of course, this impact strongly depends on the statistical characteristics calculated. For instance, for simple functions like the mean velocity and its variance n_0 can be taken relatively small; in our calculations we conclude that $n_0 = 10$ and $n_0 = 40$ lead to practically the same results. However for more complicated functions, n_0 should be taken much larger; for example, for the velocity correlation function we have taken n_0 equal to 100 and higher.

3 Simulation results

In this section we present the simulation results for the Eulerian and Lagrangian statistical characteristics, and compare our results with the data reported in [26]. We recall that the problem is considered in the dimensionless form where the correlation length scale equals to 1.

3.1 The Eulerian velocity

Let $\mathbf{v}(x,y) = (u(x,y), v(x,y))$ be the Eulerian velocity field. We calculate the mean velocities $\langle u\rangle$, $\langle v\rangle$, and the variances $\sigma_u^2 = \langle u'^2\rangle = \langle u^2\rangle - \langle u\rangle^2$, $\sigma_v^2 = \langle v'^2\rangle = \langle v^2\rangle - \langle v\rangle^2$, where $u' = u - \langle u\rangle$, $v' = v - \langle v\rangle$, and

$$B_1(x,x';y) = \langle u'(x+x',y)u'(x',y)\rangle, \quad B_2(x,x';y) = \langle v'(x+x',y)v'(x',y)\rangle,$$

are the Eulerian correlation functions of the longitudinal and transverse velocities, respectively.

We assume that the layer is long enough, so in our calculations we have taken $L_x \sim 1000$, and $L_y \sim 1 - 32$. The flow can be obviously considered as approximately horizontally homogeneous in a core region which is defined as $D_0 = \{(x,y) \in D : \ a \le x \le L_x - a\}$, where a is about of several units. In our calculations we have found that $a = 10$ was sufficient to have the horizontal homogeneity in the core region D_0.

In the core region, we have calculated the mean velocities and the variances. So due to homogeneity, these functions depend only on the transverse coordinate y. This property was conveniently used in our calculations to improve the accuracy of evaluation of the averages by taking an additional space averaging over the longitudinal direction in the core region, from a to $L_x - a$. So the total statistical error is proportional to $(N_{MC}\, L_x)^{-1/2}$ where N_{MC} is the number of Monte Carlo samples.

In the case of correlation functions, the horizontal homogeneity means that $B_i(x, x+\rho; y) = B_i(\rho, y)$, i.e., horizontally, the correlation functions depend on the difference $\rho = x - x'$. The space averaging is made here a bit more complicated. For a fixed ρ, the sum is taken over the two sets of points, $a, a+1, \ldots, a+n_p-1$, and $a+\rho, a+1+\rho, \ldots, a+n_p-1+\rho$ as follows: $\frac{1}{n_p}\sum\limits_{i=0}^{n_p-1} u(a+i,y)\, u(a+i+\rho,y)$, where n_p is an integer number which we usually take equal to $L_x/10$. The statistical error of such an averaging combined with the ensemble averaging is proportional to $(n_p\, N_{MC})^{-1/2}$.

3.2 Lagrangian statistical characteristics

The Lagrangian statistical characteristics are the most important functions in the analysis of the particle transport. In particular, often used are the mean Lagrangian velocity of a particle, the dispersion coefficient, the Lagrangian correlation function of the longitudinal and transverse velocities, and the Lagrangian probability density function (pdf) of the particle displacement, so in our calculations, we focus on these quantities.

Let us define these statistical characteristics. We denote by $\mathbf{x}_0$ the starting coordinate of a fluid particle whose Lagrangian trajectory is $\mathbf{X}(t;\mathbf{x}_0)$, $t \ge 0$, and $\mathbf{V}(t;\mathbf{x}_0) = (V_x(t;\mathbf{x}_0), V_y(t;\mathbf{x}_0)) = \mathbf{u}(\mathbf{X}(t;\mathbf{x}_0))$ is the Lagrangian velocity. By definition, $\mathbf{X}(t;\mathbf{x}_0)$ solves the following problem

$$\frac{d\mathbf{X}}{dt} = \mathbf{u}(\mathbf{X}),\ t > 0; \quad \mathbf{X}(0) = \mathbf{x}_0. \tag{16}$$

The Lagrangian processes $\mathbf{X}(t;\mathbf{x}_0)$ and $(V_x(t;\mathbf{x}_0),\, V_y(t;\mathbf{x}_0))$ depend on the starting point $\mathbf{x}_0$, i.e., on $\mathbf{x}_0 = (x_0,\, y_0)$. As to the boundary conditions, the trajectory is reflected on the left and right boundaries of the core region, while the upper and bottom boundaries are not reachable by the trajectories due to the no flow condition. In the numerical scheme, the Lagrangian trajectory can reach the upper and bottom boundaries. In these cases, we take a mirror reflection into the core region. For solving the equation (16), we used a simple Euler scheme: $\mathbf{X}(t+\Delta t) = \mathbf{X}(t) + \mathbf{u}(\mathbf{X}(t))\,\Delta t$ where the integration step was taken equal to $\Delta t = h/10$. To calculate the velocities for points inside the mesh we use a bilinear interpolation (e.g., see [15]).

Now we define the main Lagrangian statistical characteristics we deal with in this paper. Let $(x_0,\, y_0)$ be the starting point of a Lagrangian trajectory. In what follows we denote by $X(t;x_0,y_0)$ the longitudinal coordinate of the Lagrangian trajectory $\mathbf{X}(t;x_0,y_0)$. The mean displacement in the longitudinal direction is $\langle \Delta X(t;x_0,\, y_0)\rangle = \langle X(t;x_0,\, y_0)\rangle - x_0$, and $\langle X'^2(t;x_0,\, y_0)\rangle$ is its variance. The longitudinal dispersion coefficient, $k(t;x_0,y_0)$ is defined as

$$k(t;x_0,y_0) = \frac{1}{2}\frac{d\,\langle X'^2(t;x_0,\, y_0)\rangle}{dt} = \langle X'(t;x_0,\, y_0)\cdot V_x'(t;x_0,\, y_0)\rangle.$$

The Lagrangian correlation functions of the longitudinal and transverse velocities are denoted by $B_1^{(L)}(t;x_0,y_0) = \langle V_x'(t;x_0,y_0)V_x'(0;x_0,y_0)\rangle$, and
$B_2^{(L)}(t;x_0,y_0) = \langle V_y'(t;x_0,y_0)V_y'(0;x_0,y_0)\rangle$, respectively. Here $X' = X - \langle X\rangle$, and $V' = V - \langle V\rangle$. We consider also the normalized Lagrangian correlation functions:

$$R_1^{(L)}(t;x_0,y_0) = \frac{B_1^{(L)}(t;x_0,y_0)}{\left(\langle V_x'^2(t;x_0,y_0)\rangle\langle V_x'^2(0;x_0,y_0)\rangle\right)^{1/2}}\ , \tag{17}$$

$$R_2^{(L)}(t;x_0,y_0) = \frac{B_2^{(L)}(t;x_0,y_0)}{\left(\langle V_y'^2(t;x_0,y_0)\rangle\langle V_y'^2(0;x_0,y_0)\rangle\right)^{1/2}}\ , \tag{18}$$

and the Lagrangian pdf $p_L(y;t,x_0,y_0)$ defined as the probability density that a Lagrangian particle started at the point y_0 reaches the point y after the travel time t.

Note that due to the horizontal homogeneity, the above Lagrangian statistical characteristics do not depend on the longitudinal coordinate of the starting position x_0 in the core region. So it remains the dependence on the transverse coordinate of the starting position y_0, and we will write $k(t;y_0)$ for the dispersion coefficient, $p_L(y;t,y_0)$ for the Lagrangian pdf of the transverse coordinate, and $R_i^{(L)}(t;y_0)$ for the normalized Lagrangian correlation functions.

Here we also used the additional averaging over the set of Lagrangian trajectories with starting points whose longitudinal coordinates are $a, a+1, \ldots, a+n_p-1$, with a fixed vertical coordinate.

3.3 Validation

To validate our stochastic simulation algorithm we first check the conservation law, and then compare our calculations with the results due to Trefry et al. [26]. In all calculations, except for the simulations presented in the last two figures, (Figures 11 and 12) we used the Gaussian correlation function (6).

So let us start with the conservation law which has the form of continuity equation (2). From this equation and the no flow conditions on the upper and lower borders of D one can derive the

following important property: the cross averaged longitudinal velocity

$$U_x(x) = \frac{1}{L_y}\int_0^{L_y} u(x,y)\,dy$$

is constant. The value of this constant depends on the parameters L_x, L_y, σ_Y. It may also vary from one sample to another.

The finite-difference counterpart of U_x is:

$$U_{h,i} = \frac{1}{L_y}\big(\frac{h_y}{2}\,u_{i+1/2,\,1} + \sum_{j=2}^{N_y-1} h_y\,u_{i+1/2,\,j} + \frac{h_y}{2}\,u_{i+1/2,\,N_y}\big), \quad i = 1, ..., N_x - 1.$$

Indeed, multiplying the equation (9) by h_y, and the equations (10)-(11) by $h_y/2$, and then taking the sum, we get $U_{h,i} = U_{h,i-1}$, $i = 2, ..., N_x - 1$, hence $U_{h,i}$ does not depend on i. Thus the numerically calculated cross averaged longitudinal fluxes should be all equal, to within the error of calculations. The quadrature formula we used to calculate $U_{h,i}$ is based on the trapezoidal rule, which conserves exactly the cross averaged finite-difference flux $U_{h,i}$. Notice that the rectangular quadrature formula does not have this nice property.

This property was used to validate our numerical scheme. In our calculations, the quantities $U_{h,i}$, $i = 1, \ldots, N_x - 1$, which theoretically should be all equal, were varying around the mean to within a relative error of order 10^{-10}. The high accuracy is explained by the fact that we have used a direct solver for sparse systems.

Another validation can be carried out on the basis that the mean transverse velocity $\langle v\rangle$ should be zero. Indeed, from the continuity equation (2) we get

$$\frac{\partial}{\partial x}\langle u(x,y)\rangle + \frac{\partial}{\partial y}\langle v(x,y)\rangle = 0. \tag{19}$$

In the core region D_0, the mean $\langle u(x,y)\rangle$ does not depend on x, hence from (19) it follows that $\langle v(x,y)\rangle = Const$. From this, using the no flow condition $v(x,0) = 0$ we conclude that the constant in the right-hand side of the last equality vanishes, i.e., $\langle v(x,y)\rangle = 0$ for all $y \in [0, L_y]$. Our calculations confirm this conclusion with high accuracy.

Let us present a comparison of our calculations with the results reported in [26] where the flow was simulated in the region $D = [0, 256] \times [0, 64]$, the grid step was taken as $h = h_x = h_y = 1/8$. In Figure 1 we show the mean longitudinal velocity $\langle u\rangle$ (left panel) and the root mean square (rms) σ_u (right panel), as functions of y, for different values of σ_Y: $\sigma_Y = 0.5$, 1, $\sqrt{2.5}$, 2. The number of the Monte Carlo samples was $N_{MC} = 1000$, combined with the space averaging along the longitudinal direction, in the interval [10, 246]. In Figure 2 (left panel) we plot σ_v, rms of the transverse velocity, versus the transverse coordinate y.

These results clearly show that the flow is not only horizontally homogeneous in the core region, but homogeneous with respect to both coordinates in an inner part of the core region $D_1 \subset D_0$ which is separated from the upper and bottom boundaries by a distance of several correlation lengths. Notice that the region D_1 where the flow is homogeneous becomes thinner (in the vertical direction) as σ_Y increases. It is also seen that if we take the region D_1 by separating at the distance of about 10 correlation lengths, the homogeneity is ensured for all considered values of σ_v. This makes possible to evaluate the statistical characteristics $\langle u\rangle$, σ_u^2, and σ_v^2 with high accuracy by taking both the spatial averaging over D_1 and ensemble averaging over $N_{MC} = 1000$ samples.

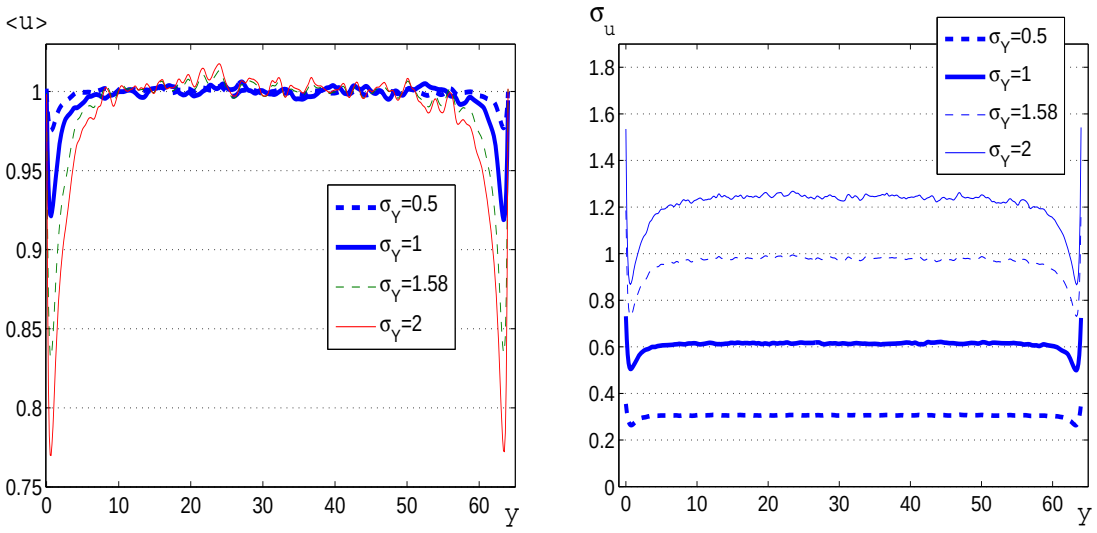

Figure 1: The mean longitudinal velocity $\langle u \rangle$ (left panel), and its root mean square σ_u (right panel) versus the transverse coordinate y, for four values of σ_Y. Sizes: $L_x = 256$, $L_y = 64$, grid step $h = 1/8$, MC statistics $N_{MC} = 1000$.

The results presented in the Figure 1 and in the left panel of Figure 2 show that the mean velocity is constant in the inner core region D_1 while the relevant rms σ_u and σ_v are monotonically increasing as σ_Y increases.

In the right panel of Figure 2 we plot the mean longitudinal velocity versus σ_Y^2 (which theoretically should be a constant), obtained by our calculations, and compared against the results reported in [26] which we present in a nondimensional form. Both results confirm that the mean velocity is practically independent of the variance of the log conductivity. More stable results of our calculations are explained by the method of combined averaging we used. Analogous comparisons are also given in Figure 3 for σ_u^2 and σ_v^2. Thus our calculations are in a good agreement with the results of [26].

3.4 Eulerian statistical characteristics of the velocity field

We are dealing with the problem of long-range transport in the horizontally stretched layer where the length is about 1000 correlation lengths, so the typical values chosen were $L_x \sim 1000$, $L_y \sim 1 - 10$. We study the flow in the core region D_0 where the velocity field can be considered horizontally homogeneous. It is therefore to expect a diffusion regime in the longitudinal direction, so we focus on the longitudinal correlations of the flow field.

It should be mentioned that to ensure that we have reached stable results we have carried out the simulations for $L_x = 200, 500, 1000$, and 6000. The results show that the statistical characteristics of the flow were practically not changing after L_x reaches 1000, so we have fixed $L_x = 1000$ in our calculations.

We present now the calculation results for the vertical profiles of the mean longitudinal velocity, the root mean squares of the transverse and longitudinal velocities, and the longitudinal behaviour of the normalized correlation functions of the Eulerian velocities defined by $R_i(\rho; y) = B_i(\rho; y)/B_i(0; y)$.

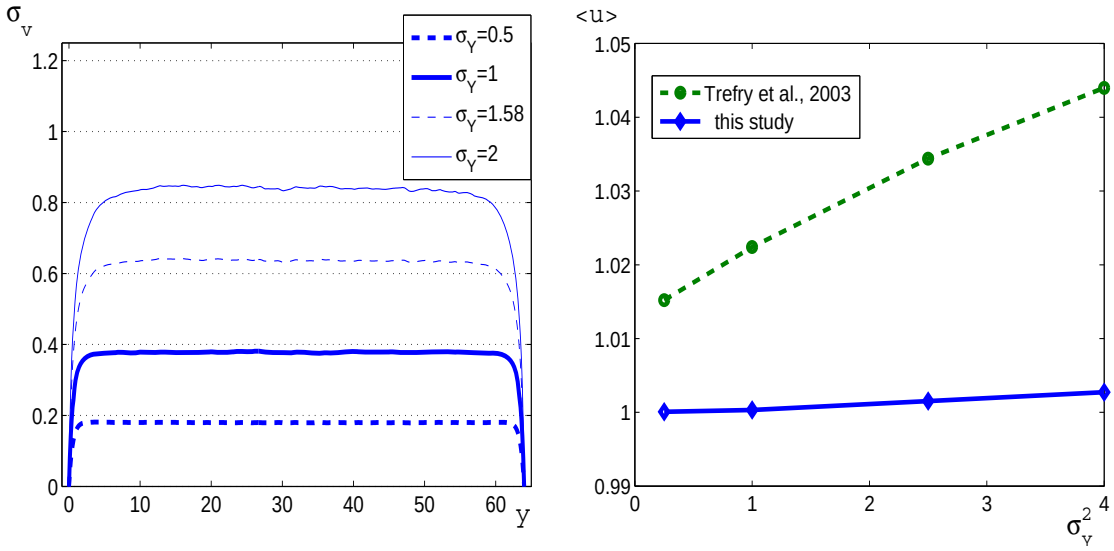

Figure 2: Left panel: the root mean square of the transverse velocity σ_v versus the transverse coordinate y, for four values of σ_Y. Right panel: the mean longitudinal velocity $\langle u \rangle$ versus σ_Y^2. Sizes: $L_x = 256$, $L_y = 64$, grid step $h = 1/8$, MC statistics $N_{MC} = 1000$.

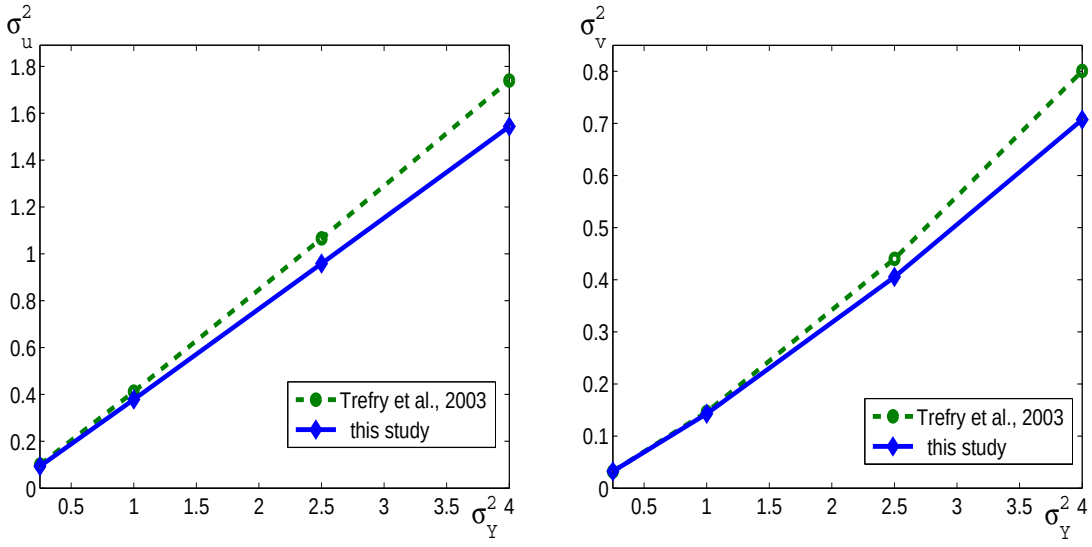

Figure 3: The variances of longitudinal velocity, σ_u^2 (left panel) and the transverse velocity,σ_v^2 (right panel) versus σ_Y^2. Sizes: $L_x = 256$, $L_y = 64$, grid step $h = 1/8$, MC statistics $N_{MC} = 1000$.

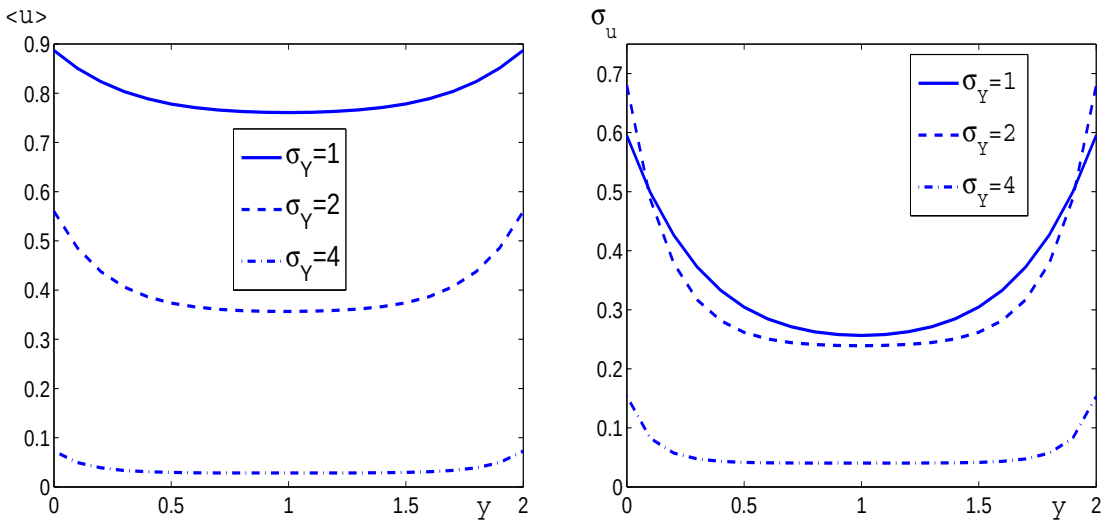

Figure 4: The mean longitudinal velocity $\langle u \rangle$ (left panel) and its rms σ_u (right panel) as functions of the transverse coordinate y for different values of σ_Y; $L_x = 1000$, $L_y = 2$, $h = 0.1$, $N_{MC} = 2500$.

In Figure 4 we plot the mean longitudinal velocity $\langle u \rangle$ (left panel) and the rms σ_u (right panel) as functions of the transverse coordinate y, for different values of σ_Y, and $L_x = 1000$, $L_y = 2$.

From these curves we can make the following conclusions: (1) the velocity field is inhomogeneous in the vertical direction, (2) the mean velocity $\langle u \rangle$ is decreasing as the variance of the log conductivity is increasing (the same for the rms, see the right panel of Figure 4). The same behaviour for σ_v is seen in the left panel of Figure 5. For large values of σ_Y (see the curves for $\sigma_Y = 4$) the transverse profiles of all these curves are getting more uniform. Note that when compared to the relevant results calculated for a thick layer (see the comments to the Figures 1, 2) we notice that the character of the transmission of the horizontal flux is different: for thick layers, the mean flux is almost constant, while for the thin layer it is decresaing with the increase of the log conductivity variance. Note also that thick and thin layers show an opposite character of the velocity fluctuations: in thick layers, the fluctuations increase with the increase of σ_Y, while in thin layers, they are decreasing. This can be seen by comparing the results of Figure 1, right panel, and Figure 2, left panel, with the results presented in the Figure 4, right panel, and Figure 5, left panel. It should be however noticed that when we turn to the fluctuation intensity $I_u = \sigma_u / \langle u \rangle$, then for both thin and thick layers, I_u increases as σ_Y increases.

In the right panel of Figure 5 the normalized correlation functions of the longitudinal $R_1(\rho; y)$ and transverse velocity $R_2(\rho; y)$ are plotted versus the longitudinal displacement ρ, along the line $y = 1$. A remarkable property in the behaviour of $R_1(\rho; y)$ is that the correlations do not vanish, and tend to a constant which is increasing with the increase of the variance of the log conductivity. It should be noted that this long-range correlation property holds also for other values of y, but at $y = 1$ it is more pronounced. This can be explained by the conservation law which ensures that the cross averaged longitudinal velocity U_x does not depend on x, hence they are 100% correlated. The vanishing correlations however would imply that the corresponding cross-averaged velocities would also tend to decorrelate which is not the case.

Another feature of $R_2(\rho; y)$ structure is the appearance of negative correlations which indicate the vertical exchange of vortices of a horizontal size compared with the correlation length scale of

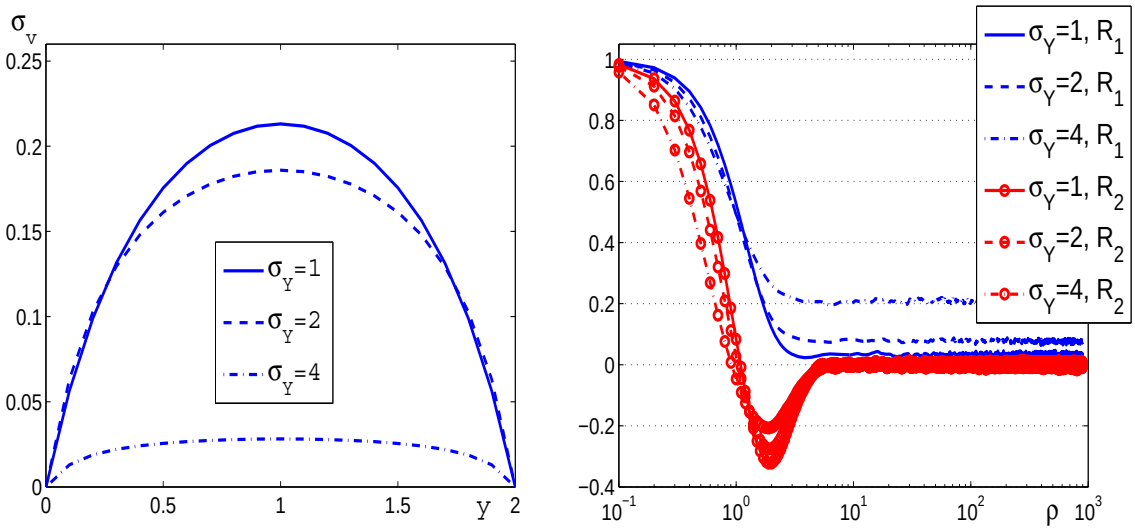

Figure 5: Left panel: rms of transverse velocity, σ_v as a function of the transverse coordinate y for different values of σ_Y. Right panel: normalized Eulerian correlation function of the longitudinal velocity, R_1 (non-marked curves), and the transverse velocity, R_2 (marked curves) versus the longitudinal displacement ρ along the line $y = 1$, for different values of σ_Y; $L_x = 1000$, $L_y = 2$, $h = 0.1$, $N_{MC} = 2500$.

log conductivity. Note that with the increase of the variance of Y the intensity of this exchange decreases.

So far we have presented the results for $L_y = 2$. We have made the above reported simulations also for layers with $L_y = 1, 4, 8$ and 32, where we have taken $h = 0.1$, and the number of Monte Carlo samples was $N_{MC} = 2500$ except for the case $L_y = 32$ where $h = 0.2$ and $N_{MC} = 1500$ were chosen. In Figure 6 we present the mean longitudinal velocity (left panel) and the relevant rms (right panel) for different values of L_y versus y/L_y. It is clearly seen that with the increase of the vertical length L_y there appears a region in the center of the flow where it becomes homogeneous. Moreover, with the increase of L_y, the mean velocity tends to its asymptotic value equal to 1.

It is interesting to notice that the increase of rms' σ_u and σ_v with the increase of L_y (see Figure 6, right panel, and Figure 7, left panel) to the asymptotic value is stabilized after $L_y = 32$, compare the relevant curves in Figure 1, right panel, and Figure 2, left panel.

As to the function $R_1(\rho; y)$, it is seen from the Figure 7, right panel, that the asymptotic values of the correlation function at large values of ρ become smaller as L_y increases. The transverse correlation function $R_2(\rho; y)$ is also presented in this panel. It is seen that with the increase of L_y the minimal values increase while the interval of the negative correlations is broadened, and the functions $R_2(\rho; y)$ tend to one stable curve.

3.5 Lagrangian statistical characteristics of the velocity field

In this section we deal with the transport problem where the main focus is the question weather there is a diffusion regime in the longitudinal direction. To study the vertical mixing of the flow we analyze the probability distribution functions of the transverse coordinate of the Lagrangian trajectories.

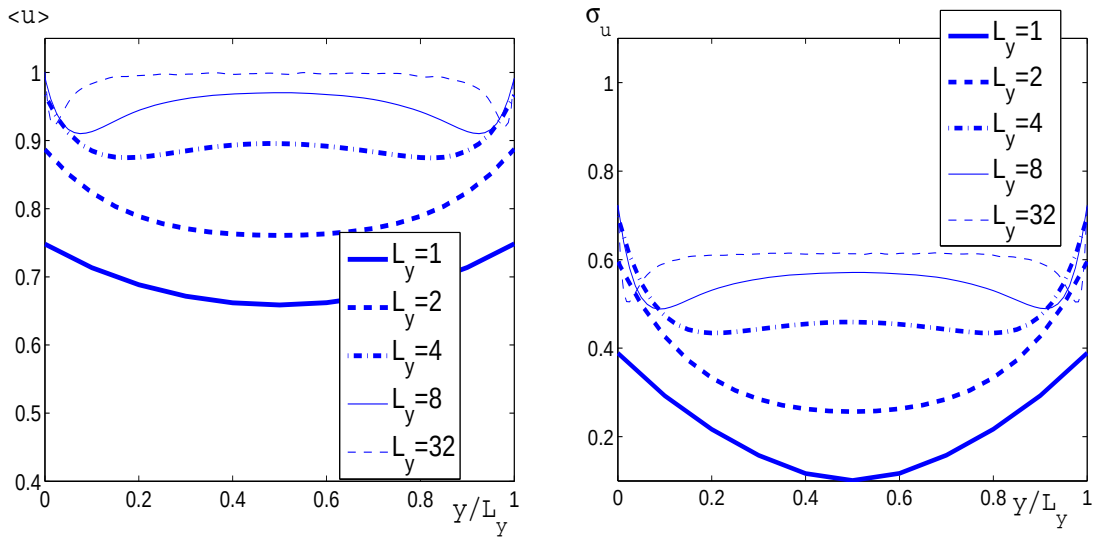

Figure 6: The mean longitudinal velocity $\langle u \rangle$ (left panel) and its rms σ_u (right panel) as functions of the normalized transverse coordinate y/L_y for different values of L_y; $L_x = 1000$, $\sigma_Y = 1$, $h = 0.1$, $N_{MC} = 2500$.

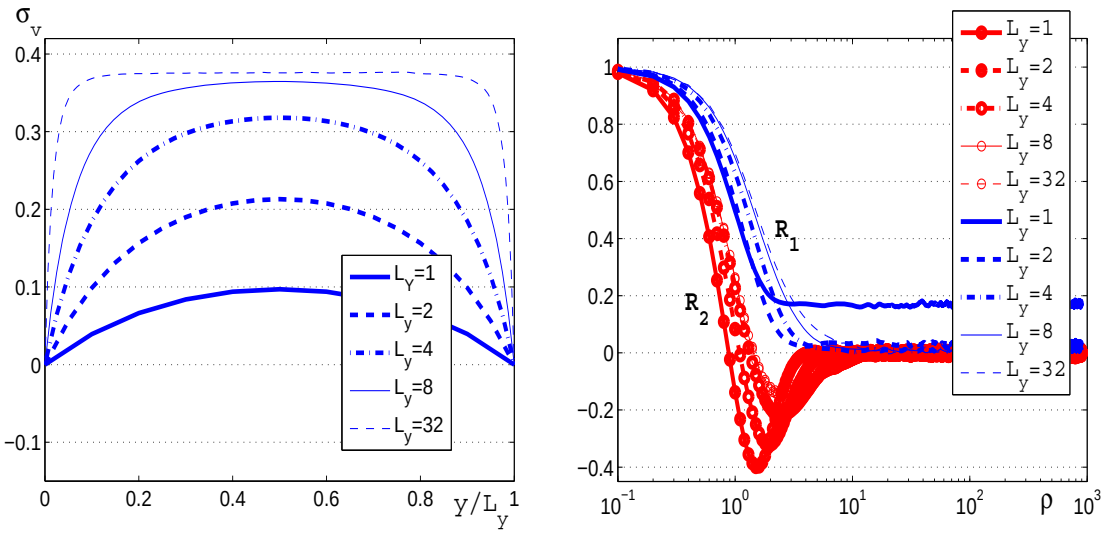

Figure 7: Left panel: rms of the transverse velocity, σ_v as a function of the normalized transverse coordinate y/L_y for different values of L_y. Right panel: normalized Eulerian correlation function of the longitudinal velocity, R_1 (nonmarked curves) and the transverse velocity, R_2 (marked curves) versus the longitudinal displacement ρ along the line $y = L_y/2$ for different values of L_y; $L_x = 1000$, $\sigma_Y = 1$, $h = 0.1$, $N_{MC} = 2500$.

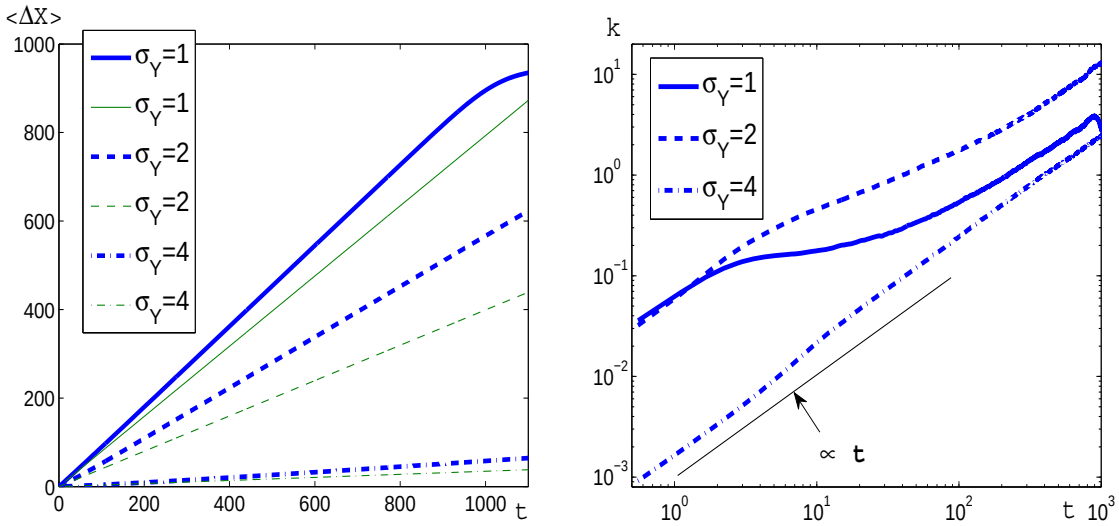

Figure 8: Left panel: the mean longitudinal displacement $\langle \Delta X(t; x_0, y_0) \rangle$ for $y_0 = 1$ (boldface lines) and lines $\langle U_x \rangle t$ (thin lines) for different values of σ_Y, as functions of travel time t; Right panel: the longitudinal dispersion coefficient $k(t; y_0)$ for $y_0 = 1$, as a function of travel time t, for different values of σ_Y. In both panels, the starting position is $y_0 = 1$. The straight line $\propto t$ is plotted to compare the curves with the linear law. The sizes $L_x = 1000$, $L_y = 2$, step $h = 0.1$, and $N_{MC} = 2500$.

In Figure 8, left panel, the mean longitudinal displacements are presented as functions of the travel time for different values of σ_Y (boldface curves). For comparison, thin lines of the form $\langle U_x \rangle\, t$ are shown. Notice that the tangent of the boldface curves is the mean of the Lagrangian longitudinal velocity, and of the thin lines, it is the mean of the cross averaged Eulerian velocity. From these plots we see the well expected linear law for the mean displacement thus the mean Lagrangian longitudinal velocity becomes independent of time. More interesting is the effect that the mean Lagrangian longitudinal velocity is larger than the mean of the cross averaged Eulerian velocity $\langle U_x \rangle$. This can be explained by the transverse inhomogeneity of the flow. It should be added that this effect becomes less pronounced for thicker layers. Notice by the way that the curve $\langle \Delta X(t) \rangle$ for $\sigma_Y = 1$ on the Figure 8, left panel, has a small region at the end of the time interval where it starts to deviate from the straight line. This is explained by the fact that in the case $\sigma_Y = 1$ the particles reach the right end of the core region faster, and then, they are stopped there.

Let us discuss now the problem of an existence of a diffusion regime in the longitudinal dispersion. The existence of a diffusion regime means that there is a time interval, which is assumed to be large enough, where the dispersion $\langle X'^2(t) \rangle$ becomes a linear function of time. This in turn implies that the dispersion coefficient $k(t)$ tends to a constant value.

Let us recall the well known formula which relates the dispersion coefficient $k(t)$ and the Lagrangian correlation function of the velocity [14]

$$k(t) = \int_0^t B_1^{(L)}(\tau)\, d\tau = B_1^{(L)}(0) \int_0^t R_1^{(L)}(\tau)\, d\tau \tag{20}$$

which is true if the Lagrangian velocity is a stationary random process.

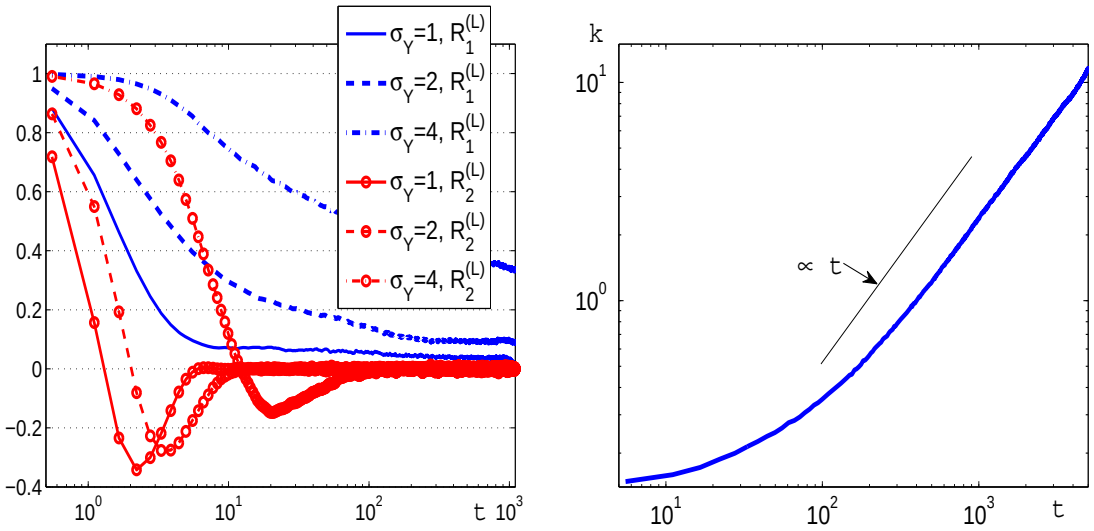

Figure 9: Left panel: The normalized Lagrangian correlation function of the longitudinal velocity, $R_1^{(L)}(t;y_0)$ (non marked curves) and the transverse velocity, $R_2^{(L)}(t;y_0)$ (marked curves) for $y_0 = 1$ as functions of travel time t, for different values of σ_Y; The sizes $L_x = 1000$, $L_y = 2$, step $h = 0.1$, and $N_{MC} = 2500$. Right panel: the longitudinal dispersion coefficient $k(t;y_0)$ for $y_0 = 1$, as a function of travel time t; $L_x = 6000$, $L_y = 2$, $\sigma_Y = 1$, $h = 0.1$, $N_{MC} = 1000$.

We deal with a quite long time interval, $(0, 10^3)$, so the longitudinal Lagrangian velocity $V_x(t)$ can be considered as an approximately stationary process, of course, beginning from a time t_1 which is large enough. So keeping in mind the relation (20), let us analyze the curves in Figure 8, right panel, and Figure 9, left panel. In Figure 8, right panel, we present the dispersion coefficient $k(t)$ as a function of time for three different values of σ_Y. The behaviour of these curves is not simple to explain: for $\sigma_Y = 2$ and $\sigma_Y = 4$ there is no evidence of a diffusion regime; for $\sigma_Y = 1$ there appears a time interval $(2, 20)$ where $k(t)$ is little varying, but for $t > 20$ it starts again to increase. Let us give a possible explanation of this interesting behaviour.

The monotonic increase of $k(t)$ for $\sigma_Y = 4$ on the whole time interval can be understood when looking at the relevant curve $R_1^{(L)}$ in Figure 9, left panel. Indeed, the long and heavy tail of $R_1^{(L)}$ gives a considerable contribution to the integral in the representation (20). The same is true for the case $\sigma_Y = 2$ but the contribution is smaller since the tail of $R_1^{(L)}$ is not so heavy. As to the case $\sigma_Y = 1$, it is of particular interest. Here the tail is relatively light, and during a certain time the correlations are almost not increasing, but after the time instant $t \sim 20$ the contribution leads to a new increasing of the correlations.

Note that the discussed long and heavy tails of $R_1^{(L)}$ and the features of the dependence of $R_1^{(L)}$ on σ_Y are similar to that of the correlation R_1 of the Eulerian velocity. The main difference, which is important for transport phenomena, is that the tails of $R_1^{(L)}$ are lying higher that the tails of R_1 which implies that the long correlations have a more pronounced impact on the Lagrangian correlations and hence on the long-range transport.

One may suspect that the time interval $(0, 10^3)$ was not large enough to ensure an appearing of the diffusion regime. We have made calculations of $k(t)$ for the time interval $(0, 5500)$, see Figure 9, right panel. These results confirm that there is no diffusion regime in the longitudinal dispersion. So we conclude that we deal here with an anomalous diffusion which is in the considered case a

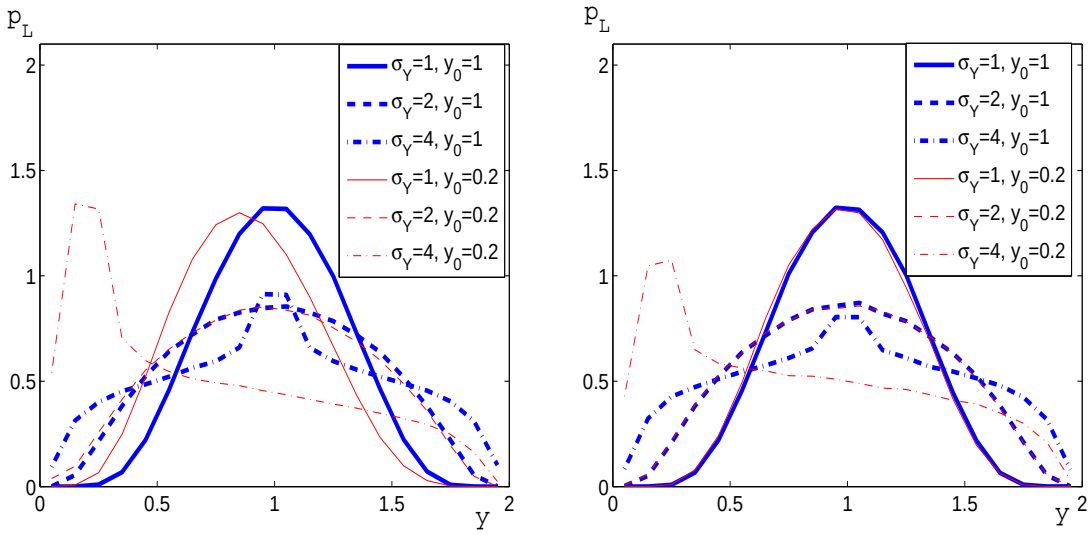

Figure 10: The probability density function of the transverse coordinate, $p_L(y;t,y_0)$ for $y_0 = 1$ (boldface line) and $y_0 = 0.2$ (thin line), for the travel time $t = 400$ (left panel) and $t = 800$ (right panel) as functions of the transverse coordinate y, for different values of σ_Y; the sizes $L_x = 1000$, $L_y = 2$, step $h = 0.1$, and $N_{MC} = 2500$.

superdiffusion with the dependence $\langle X'^2(t)\rangle \sim c\,t^2$ true for the time intervals large enough.

Let us discuss the transverse mixing of particles in the layer. It is convenient to characterize the transverse mixing by the transition probability density function $p_L(y;t,y_0)$ which is the probability density that a Lagrangian particle started at the point y_0 reaches the point y after the travel time t. In Figure 10 we plot the function $p_L(y;t,y_0)$ for two starting positions, $y_0 = 0.2$ (close to the bottom), and $y_0 = 1$ (center of the layer), for the time $t = 400$ (left panel), and $t = 800$ (right panel).

It is reasonable to say that the particles become well mixed in the transverse direction if the function $p_L(y;t,y_0)$ looses its dependence on y_0, i.e., the Lagrangian particle has forgotten its starting position y_0. So in our calculations, it means that the pdf's of our two particles become almost coincident. From the Figure 10, left panel, it is seen that to the time $t = 400$, for $\sigma_Y = 2$, the mixing is obvious, while for $\sigma_Y = 1$ and $\sigma_Y = 4$, this is not the case. To the time $t = 800$, the mixing happens for $\sigma_Y = 1$, too, but for $\sigma_Y = 4$ there is no mixing.

A remarkable feature of the steady state density p_L is that unexpectedly, it is not uniform over the transverse coordinate, even for large values of σ_Y. Recall that we discuss here the case of a thin layer of height $L_Y = 2$. For larger heights the density P_L becomes more uniform, and the mixing happens after longer times.

Another interesting property of the transverse dispersion is that the probability to reach the upper or the lower boundary of the layer is very small, and the smaller the value of σ_Y, the smaller is this probability. In a sense, the particles are pushed away from the boundaries. This is related to the transverse profiles of σ_v near the boundaries. There is an analogy with the turbulent boundary layer flows where there is a vertical exchange increasing with the distance to the boundary which leads to a non-zero vertical Lagrangian velocity pushing the particles away from the boundary (e.g., see [14]).

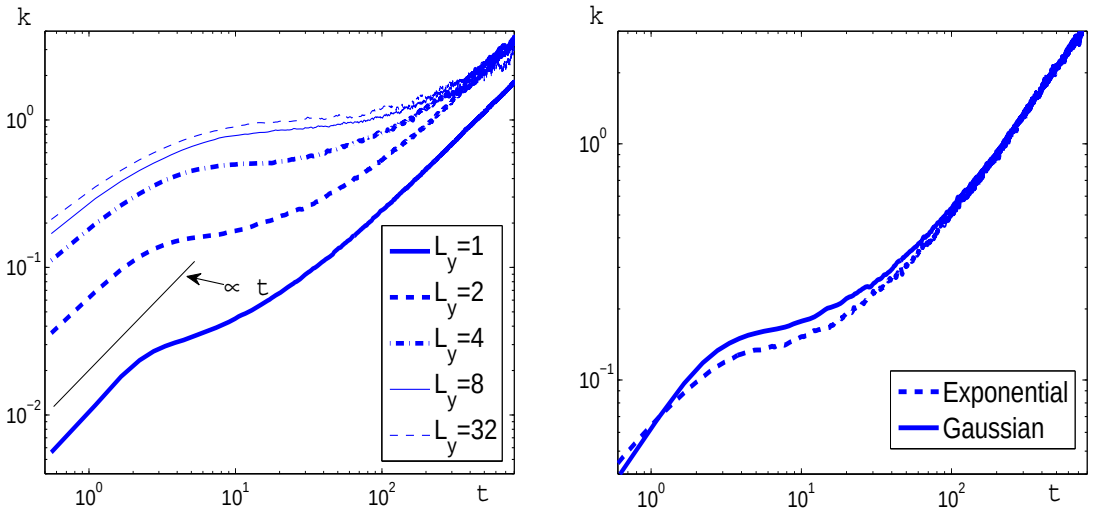

Figure 11: Left panel: the longitudinal dispersion coefficient $k(t; y_0)$ for $y_0 = L_y/2$ as a function of travel time t, for different values of L_y; $L_x = 1000$, $\sigma_Y = 1$, $h = 0.1$, $N_{MC} = 2500$. Right panel: the dispersion coefficient $k(t; y_0)$ for $y_0 = 1$ as a function of the travel time t, for exponential and Gaussian correlation functions; $L_x = 1000$, $L_y = 2$, $\sigma_Y = 1$, $h = 0.1$, $N_{MC} = 2500$.

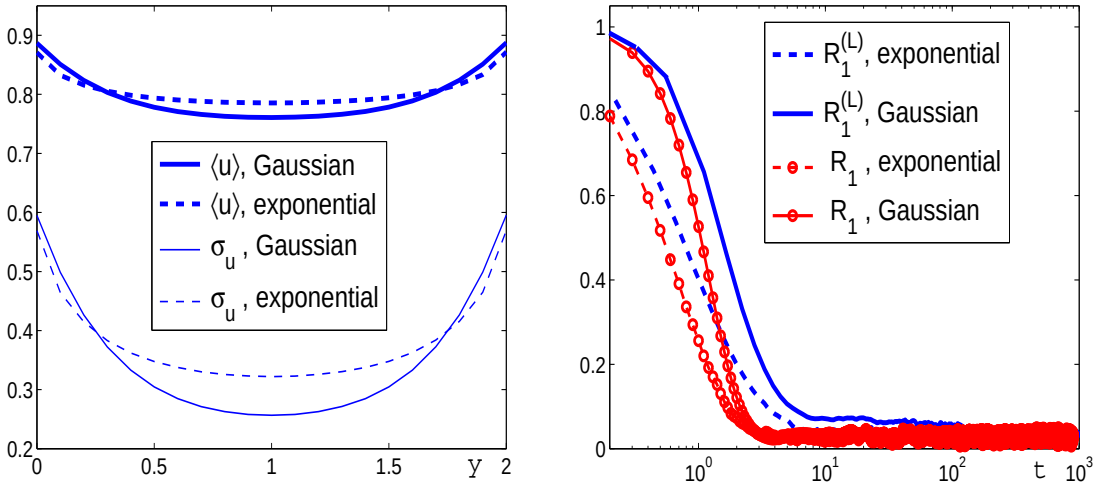

Figure 12: Left panel: the mean longitudinal velocity $\langle u \rangle$ and its rms σ_u as functions of the transverse coordinate y for log conductivity with exponential and Gaussian correlation functions. Right panel: normalized Eulerian, R_1 and Lagrangian, $R_1^{(L)}$ correlation functions of the longitudinal velocity for $y_0 = 1$, as functions of the travel time t. For both panels $L_x = 1000$, $L_y = 2$, $\sigma_Y = 1$, $h = 0.1$, $N_{MC} = 2500$.

As already mentioned we have carried out calculations also for larger heights of the layer. We were expecting to observe a diffusion regime as the layer height increases. This is generally true but even for heights up to 32 there was no clear diffusion regime, see Figure 11, left panel. For larger heights, the time interval where the diffusion regime exists is getting broader.

Finally we mention that all the above simulation results were carried out for the Gaussian correlation function of Y, but the main conclusions were confirmed in our simulation with the exponential correlation function. In Figure 11, right panel, we show a comparison of $k(t)$ for these two cases. It is seen that the difference is quite small. As to the mean velocities, variances, and the correlation functions, (see the comparison presented in Figure 12), there are some differences which however do not change our conclusions about the anomalous diffusion and long-range correlations.

In conclusion let us give the information on the computer resources used in our calculations. The simulations have been carried out on the Workstation HP BL 480C with processor Dual Core Intel Xeon 5160 (3Ghz) and 24 Gbt RAM. A characteristic time of the flow simulation for a grid of 10^6 nodes has taken about of 1 minute. The cost of the method is linear increasing with the number of grid points, and for a fixed grid, it does not depend on the variance of the log conductivity.

4 Appendix: some simulation formulae

4.1 Simulation of log conductivity

Assume that a zero mean homogeneous Gaussian random field $u(\mathbf{x})$ is defined by its spectral function $F(\mathbf{k})$, $\mathbf{k} \in I\!R^d$, so that the correlation function is

$$B(\mathbf{r}) = \langle u(\mathbf{x}+\mathbf{r})u(\mathbf{x})\rangle = \int_{R^d} e^{\mathrm{i}2\pi\mathbf{k}\cdot\mathbf{r}} F(\mathbf{k})\, d\mathbf{k}.$$

The field $u(\mathbf{x})$ can be simulated by the Randomization spectral method (e.g., see [10], [13], [16]):

$$u_{n_0}(\mathbf{x}) = \frac{1}{\sqrt{n_0}} \sum_{j=1}^{n_0} \left(\frac{F(\mathbf{k}_j)}{p(\mathbf{k}_j)}\right)^{1/2} \left\{\xi_j \cos\theta_j + \xi'_j \sin\theta_j\right\} \tag{21}$$

where ξ_j, ξ'_j, $j = 1, ..., n_0$ are mutually independent, standard Gaussian random variables, $\mathbf{k}_j$, $j = 1, ..., n_0$ are mutually independent and independent of ξ_j, ξ'_j, $j = 1, ..., n_0$, d-dimensional random vectors with the common pdf $p(\mathbf{k})$ (satisfying the consistency condition $p(\mathbf{k}) > 0$ if $F(\mathbf{k}) > 0$), $\theta_j = 2\pi(\mathbf{k}_j \cdot \mathbf{x})$.

It is worth mentioning that for any n_0, the random field $u_{n_0}(\mathbf{x})$ has the desired target correlation function. To ensure that the distributions of the random field $u_{n_0}(\mathbf{x})$ are close to Gaussian one should take n_0 large enough.

It is to mention that in (21), one can take arbitrary random variables ξ_j, ξ'_j, $j = 1, ..., n_0$ satisfying the conditions

$$\langle\xi_j\rangle = \langle\xi'_j\rangle = 0, \quad \langle\xi_i\xi_j\rangle = \langle\xi'_i\xi'_j\rangle = \delta_{ij}, \qquad \langle\xi_i\xi'_j\rangle = 0.$$

For example one can choose $\xi_j = \sqrt{2}\cos(2\pi\gamma_j)$, $\xi'_j = -\sqrt{2}\sin(2\pi\gamma_j)$, where γ_j, $j = 1, ..., n_0$ are independent random variables uniformly distributed in $[0, 1]$. Then (21) can be represented in a form which is probably more conventional in the hydrogeology community (e.g., see [4])

$$u_{n_0}(\mathbf{x}) = \frac{\sqrt{2}}{\sqrt{n_0}} \sum_{j=1}^{n_0} \left(\frac{F(\mathbf{k}_j)}{p(\mathbf{k}_j)}\right)^{1/2} \cdot \cos(\theta_j + 2\pi\gamma_j). \tag{22}$$

If we apply the commonly used simulation formulae for two independent standard gaussian variables

$$\xi = \sqrt{-2\ln\gamma}\,\cos(2\pi\gamma'), \quad \xi' = \sqrt{-2\ln\gamma}\,\sin(2\pi\gamma'),$$

where γ and γ' are two independent random variables uniformly distributed on $[0,1]$, then the representation (21) can be simplified to

$$u_{n_0}(\mathbf{x}) = \frac{1}{\sqrt{n_0}} \sum_{j=1}^{n_0} \left(\frac{F(\mathbf{k}_j)}{p(\mathbf{k}_j)} \right)^{1/2} \cdot \sqrt{-2\ln\gamma_j}\,\cos(\theta_j + 2\pi\gamma'_j). \tag{23}$$

Here γ_j, γ'_j, $j = 1, ..., n_0$ are mutually independent and independent of $\mathbf{k}_j$, $j = 1, ..., n_0$, random variables uniformly distributed on $[0,1]$.

It should be mentioned that the one-point distribution of the random field model (23) is exactly Gaussian for any integer n_0. Notice that the model (22) has not this nice property.

4.2 Simulation of random fields with the Gaussian correlation function

Let $u(x_1, x_2)$ be a 2D zero mean homogeneous Gaussian random function with the Gaussian correlation function

$$B(r_1, r_2) = \sigma^2 e^{-r_1^2/\lambda_1^2 - r_2^2/\lambda_2^2}.$$

Here λ_i, $i = 1, 2$ are the correlation lengths, σ^2 is the variance. Then the spectral function of the field reads

$$F(k_1, k_2) = \sigma^2 \pi \lambda_1 \lambda_2 e^{-\pi^2(k_1^2\lambda_1^2 + k_2^2\lambda_2^2)}.$$

Let us choose

$$p(\mathbf{k}) = \pi \lambda_1 \lambda_2 e^{-\pi^2(k_1^2\lambda_1^2 + k_2^2\lambda_2^2)}.$$

Then the random vector $\mathbf{k}$ with this pdf can be simulated by the formula $\mathbf{k} = \frac{1}{\sqrt{2\pi}}(\eta/\lambda_1,\, \eta'/\lambda_2)$ where η, η' are independent standard Gaussian random variables. Therefore,

$$u(x_1, x_2) = \frac{\sigma}{\sqrt{n_0}} \sum_{j=1}^{n_0} (\xi_j \cos\tilde{\theta}_j + \xi'_j \sin\tilde{\theta}_j) \tag{24}$$

where $\tilde{\theta}_j = \sqrt{2}(\eta_j x_1/\lambda_1 + \eta'_j x_2/\lambda_2)$, and ξ_j, ξ'_j, η_j, η'_j, $(j = 1, ..., n_0)$ are mutually independent standard Gaussian random variables.

4.3 Simulation of random fields with the exponential correlation function

The correlation function $B(x, \rho) = \sigma^2 e^{-(x^2/\lambda_1^2 + \rho^2/\lambda_2^2)^{1/2}}$ has the spectral function

$$F(k_1, k_2) = 2\pi\lambda_1\lambda_2\sigma^2 \left(1 + (2\pi k_1\lambda_1)^2 + (2\pi k_2\lambda_2)^2\right)^{-3/2}.$$

If we take $p(\mathbf{k}) = 2\pi\lambda_1\lambda_2 \left(1 + (2\pi k_1\lambda_1)^2 + (2\pi k_2\lambda_2)^2\right)^{-3/2}$, then the simulation formula for $\mathbf{k} = (k_1, k_2)$ with this probability density function is $k_1 = (1/\gamma_2^2 - 1)^{1/2}\cos(2\pi\gamma_1)/(2\pi\lambda_1)$, and $k_2 = (1/\gamma_2^2 - 1)^{1/2}\sin(2\pi\gamma_1)/(2\pi\lambda_2)$, where γ_1, γ_2 are two independent random variables uniformly distributed in $[0,1]$. Therefore, the random field $u(x_1, x_2)$ with the exponential correlation

function (7) can be simulated by the formula (24) where ξ_j and ξ'_j, $j = 1, ..., n_0$ are mutually independent standard Gaussian random variables; $\tilde{\theta}_j = (1/\gamma_{2,j}^2 - 1)^{1/2}[\cos(2\pi\gamma_{1,j})\, x/\lambda_1 + \sin(2\pi\gamma_{1,j})\, \rho/\lambda_2]$, and $\gamma_{1,j}$, $\gamma_{2,j}$, $j = 1, ..., n_0$ are mutually independent and independent of ξ_j and ξ'_j, $j = 1, ..., n_0$ random variables uniformly distributed in $[0, 1]$.

It should be mentioned that the examples we present here include correlation functions with rapidly decreasing tails, thus the log conductivity length scale λ is the only one parameter which characterizes the correlation structure. In more complicated cases the correlation functions may have heavy tails, for instance decreasing according to the power law (as in the fractal media with multiscale heterogeneities, e.g., see [9]). In this cases, a detailed representation of all the scales is a difficult problem, and a modification of the Randomization spectral models called Stratified Randomization spectral models can be successfully applied (e.g., see [12] and [11]).

5 Conclusion

We have presented results of stochastic simulations of flows and particle transport in a 2D layer of random porous medium. The porous medium is characterized by a hydraulic conductivity which is assumed to be a lognormal random field. Numerical experiments are carried out by solving the Darcy equation for each sample of the random hydraulic conductivity by a direct solver for sparse systems, and tracking Lagrangian trajectories in the simulated flow.

We present a numerical analysis of different Eulerian and Lagrangian statistical characteristics of the flow such as the transverse and longitudinal velocity correlation functions, the diffusion coefficient, the mean displacement of Lagrangian particles, and the probability density function of the transverse Lagrangian coordinate.

We focus on the existence of a diffusion regime in the longitudinal dispersion. It was found that even for long layers of about 10^3 log conductivity correlation lengths and heights up to 32 correlation lengths there is no diffusion regime. This is true both for moderate ($\sigma_Y \sim 1$) and large ($\sigma_Y \sim 4$) fluctuations of the log conductivity. This is related to the long and heavy tails of the correlation functions of the longitudinal velocities which in turn is related to the divergence free property of the velocity field, and to the no flow boundary conditions.

Important feature of the flow is that the steady state mean Lagrangian longitudinal velocity is higher than the mean cross averaged Eulerian longitudinal velocity. This effect is more pronounced for larger fluctuation intensities of log conductivity, and less pronounced for thicker layers.

The impact of the intensity of log conductivity fluctuations on the flow is different for thick and thin layers. In the case of thin layers with the height compared to one correlation length, an increase of the log conductivity fluctuations leads to a decreasing of the mean and variance of the longitudinal velocity. For thick layers this dependence is converse.

A remarkable feature of the transverse mixing of particles is that even after thousands of correlation times the transverse distribution is not uniform, having a stable transverse profile. This is caused by the no flow boundary conditions and the relevant vertical gradient of the transverse velocity variance.

Finally we remark that we believe that the main conclusions of this study remain true also for 3D layers, but in some details the long-term transport in 3D flows may be of course different, so we are going to made the relevant 3D simulations.

References

[1] Rachid Ababou, Dennis McLaughlin, Lynn W. Gelhar and Andrew F.B. Tompson. Numerical simulation of three-dimensional saturated flow in randomly heterogeneous porous media. *Transport in Porous Media*, **4** (1989), N 6, 549-565.

[2] G. Dagan. *Flow and Transport in Porous Formations.* Springer-Verlag, Berlin-Heidelberg, Germany, 1989.

[3] G. Dagan. Spatial moments, Ergodicity, and Effective Dispersion. *Water Resour. Res.,* **26** (1990), 6,1281-1290.

[4] M. Dentz, H. Kinzelbach, S. Attinger and W. Kinzelbach. Temporal Behaviour of a Solute Cloud in a Heterogeneous porous medium. 3. Numerical simulations. *Water Resour. Res.,* **38** (2002), 7, 1118-1130.

[5] Jean-Raynald Dreuzy, Anthony Beaudoin, and Jocelyne Erhel. Asymptotic dispersion in 2D heterogeneous porous media determined by parallel numerical simulations. *Water Resour. Res.*, **43** (2007), W10439.

[6] Freeze R.A. A stochastic-conceptual analysis in groundwater flow in non-uniform, homogeneous media. *Water Resour. Res.*, **11** (1975), 5, 725-741.

[7] Lynn W. Gelhar. *Stochastic Subsurface Hydrology.* Prentice-Hall, Englewood Cliffs, N.J., 1993.

[8] Roger G. Ghanem, Pol D. Spanos. *Stochastic finite elements. A spectral approach.* Courier Dover Publications, 2003.

[9] James Glimm and David H. Sharp. A random field model for anomalous diffusion in heterogeneous porous media. *Journal of Statistical Physics*, **62** (1991), N1/2, 415-424.

[10] R.H. Kraichnan. Diffusion by a random velocity field. *Phys.Fluids*, **13** (1970), N1, 22-31.

[11] P. Kramer, O. Kurbanmuradov, and K. Sabelfeld. Comparative Analysis of Multiscale Gaussian Random Field Simulation Algorithms. *Journal of Computational Physics*, **226** (2007), 897-924.

[12] O. Kurbanmuradov, K. Sabelfeld, and D. Koluhin. Stochastic Lagrangian models for two-particle motion in turbulent flows. Numerical results. *Monte Carlo Methods Appl.*, **3** (1997), 3, 199–223.

[13] Mikhailov G.A. Approximate models of random processes and fields. *Russian J. Comp. Mathem. and mathem. Physics*, vol.23 (1983), N3, 558-566. (in Russian).

[14] A.S. Monin and A.M. Yaglom. *Statistical Fluid Mechanics: Mechanics of Turbulence*, Volume 1. The MIT Press, 1971.

[15] Pollock, D.W. Semianalytical computation of path lines for finite-difference models, *Ground Water.Res.*, **28** (1988), 743-750.

[16] Sabelfeld, K.K. *Monte Carlo Methods in Boundary Value Problems.* Springer-Verlag, Berlin – Heidelberg – New York, 1991.

[17] K. Sabelfeld. Stokes flows under random boundary velocity excitations. *J. Stat. Physics*, accepted, 2008.

[18] Sabelfeld K. and Kolyukhin D. Stochastic Eulerian model for the flow simulation in porous media. *Monte Carlo Methods and Applications*. **9** (2003), 3, 271-290.

[19] Salandin, P., and V. Fiorotto. Solute transport in highly heterogeneous aquifers. *Water Resour. Res.*, **34** (1998), 949-961.

[20] A.A. Samarskii, E.S. Nikolaev. *Numerical Methods for Grid Equations*, Birkhauser, 1989

[21] H. Schwarze, U. Jaekel and H. Vereecken. Estimation of Macrodispersion by Different Approximation Methods for Flow and Transport in Randomly Heterogeneous Media. *Transport in Porous Media*, **49**(2001), 2, 267-287.

[22] L. Smith and R.A. Freeze. Stochastic Analysis of Steady State Groundwater Flow in a Bounded Domain, 2. Two-Dimensional Simulation. *Water Resour. Res.*, **15** (1979), 6, 1543-1559.

[23] Suciu N., C. Vamos, H. Vereecken, K. Sabelfeld, and P. Knabner, Memory Effects Induced by Dependence on Initial Conditions and Ergodicity of Transport in Heterogeneous Media, *Water Resour. Res.* **44** (2008), W08501, doi: 10.1029/2007WR006740

[24] Lei Sun, Changjun Peng, Honglai Liu, and Ying Hu. Analogy in the adsorption of random copolymers and homopolymers at solid-liquid interface: A Monte Carlo simulation study. *J. Chem. Phys.* **126** (2007), 094905; DOI:10.1063/1.2567301.

[25] Tompson, A.F.B., and L.W. Gelhar. Numerical simulation of solute transport in tree-dimensional randomly heterogeneous porous media. *Water Resour. Res.*, **26**(1990), 10, 2541-2562.

[26] M.G. Trefry, F.P. Ruan and D. McLaughlin. Numerical simulations of preasimptotic transport in hetoregenous porous media: Departures from the Gaussian limit. *Water Resour. Res.,* **39** (2003), 3, 1063-1077.

[27] Dongbin Xiu, George Em Karniadakis. The Wiener–Askey Polynomial Chaos for Stochastic Differential Equations. *SIAM Journal on Scientific Computing*, **24** (2002), 2, 619 - 644.

[28] J. Yang, D. Zhang, Z. Lu. Stochastic analysis of saturated-unsaturated flow in heterogeneous media by combining Karhunen-Loeve expansion and perturbation method. *Journal of Hydrology.* **294** (2004), 18-38.

[29] Dongxiao Zhang and Zhiming Lu. An efficient, high-order perturbation approach for flow in random porous media via Karhunen-Loeve and polynomial expansions. *Journal of Comp. Physics*, **194** (2004), 773-794.